PERGAMON

International Journal of Multiphase Flow 25 (1999) 1457–1489

International Journal of Multiphase Flow

www.elsevier.com/locate/ijmulflow

Experimental analysis and modelling of particle-wall collisions

M. Sommerfeld[a,*], N. Huber[b]

[a]*Fachbereich Ingenieurwissenschaften, Martin-Luther-Universität Halle-Wittenberg, 06099 Halle (Saale), Germany*
[b]*Siemens AG, Bereich KWU, Freyeslebenstr. 1, 91058 Erlangen, Germany*

Received 16 November 1998; received in revised form 29 April 1999

This contribution is dedicated to Professor Gad Hetsroni on the occasion of his 65th birthday.

Abstract

A detailed experimental analysis of the particle-wall collision process in a particle-laden horizontal channel flow was performed using particle tracking velocimetry. The particles used in this study were glass beads with a diameter of 100 and 500 μm and quartz particles with a size of about 100 μm. Moreover, the effect of wall material on the collision process was analysed. Special attention was paid to the influence of wall roughness and therefore, untreated stainless steel, polished stainless steel, Plexiglas, and rubber gum were used. It was found that wall roughness considerably alters the rebound behaviour of the particles and causes in average a re-dispersion of the particles, i.e. gravitational settling is reduced. A similar effect was observed for the non-spherical quartz particles and a polished stainless steel wall. The experimental data were used to improve and validate a wall collision model to be used in the frame of the Lagrangian approach. In this model the wall roughness is simulated by assuming that the impact angle is composed of the trajectory angle with respect to the plane wall and a stochastic component caused by wall roughness. A modified normal distribution function was assumed for the roughness angle distribution. All the parameters for the wall collision model, such as restitution coefficient and friction coefficient as functions of the impact angle were obtained from the experiments. The simulations showed a very good agreement with the measurements for the particle rebound properties.

Keywords: Particle-laden flow; Horizontal channel; Particle-wall collisions; Wall roughness; Non-spherical particles; Particle tracking velocimetry; Lagrangian approach; Wall collision model

* Corresponding author. Tel.: +49-(0)3461-462879; fax: +49-(0)3461-462878.
E-mail address: martin.sommerfeld@iw.uni-halle.de (M. Sommerfeld)

0301-9322/99/$ - see front matter
PII: S0301-9322(99)00047-6

1. Introduction

Confined, wall-bounded and turbulent gas-particle flows are frequently found in technical and industrial processes, such as pneumatic conveying, fluidised beds, vertical risers, particle separation in cyclones, classification of particles, and mixing devices. The motion of particles in such flows is governed by a number of physical effects, such as turbulence, gravity, transverse aerodynamic lift forces, and particle-wall collisions. At higher particle loading, collisions between particles (Sommerfeld, 1995) and the modulation of mean flow and turbulence (Kulick et al., 1994) may additionally be of relevance. The importance of particle-wall collisions is correlated with the particle inertia (i.e. the particle response distance) and the dimensions of the confinement and may be initiated by turbulence, inertial effects, and gravity in horizontal flows. The wall collision frequency has a direct effect on the pressure drop in pneumatic conveying since each collision is associated with a momentum loss of the particles, followed by its acceleration by the air flow after rebound. This acceleration extracts momentum from the fluid and hence causes an additional pressure drop. Wall roughness may considerably alter the wall collision process and the wall collision frequency as has been demonstrated previously (Tsuji et al., 1985, 1987; Sommerfeld, 1992, 1996; Frank et al., 1993; Sommerfeld et al., 1993; Sommerfeld and Huber, 1995). As observed by Sommerfeld and Huber (1995) and described in detail by Sommerfeld and Zivkovic (1992), Sommerfeld (1995), wall roughness results in a re-dispersion of particles in horizontal pipe or channel flows and tends to increase the wall collision frequency. Similar effects are caused by the non-sphericity of particles which may rebound at larger angles compared to the impact angle as a result of rotation. This effect was analysed in detail by Tsuji et al. (1991). For reliable numerical calculations of confined gas–solid flows an appropriate modelling of the collision process of spherical particles with rough walls or of non-spherical particles with smooth or rough walls is essential. Such models may be based on a purely empirical approach (e.g. Grant and Tabakoff, 1975) which requires numerous experimental studies to provide correlations which include all the relevant parameters, or on an approach which is based on principle conservation laws which are extended in some way to account for stochastic effects such as wall roughness and non-sphericity of particles (Sommerfeld, 1992). The latter approach is preferred in the present study. Hence, data are needed for various combinations of particle and wall material on the restitution coefficient and the friction coefficient.

Quite a number of experimental studies have been performed in the past in order to analyse the wall impact of solid particles and to provide data for modelling the process. Studies on plastic and elastic collisions of small glass beads with metal surfaces were performed by Martin et al. (1991) using Laser-Doppler anemometry. Two different test rigs were used in order to study low speed and high speed impact in addition to erosion phenomena. The low speed studies were performed in an evacuated drop tube, while the high speed impacts were realised by directing a particle laden jet onto the target. The velocity measurements were performed just above the target in order to allow the recording of impact and rebound velocity. The effects of both impact angle and velocity on the normal restitution ratio[1] were analysed. The

[1] The term restitution ratio is used for the measured velocity ratios parallel and normal to the wall, while the term restitution coefficient is used for the model constant relating the change of the normal velocity component.

dependence of the restitution ratio on the impact angle showed that the impact process is quite different for a hard and a soft wall. In the case of the hard wall the restitution ratio decreases from about one at zero impact angle (note that the impact and rebound angles are those between wall and particle trajectory in this case) to about 0.7 at an impact angle of 45° and then increases again to about 0.97 at normal impact. For the soft wall the restitution ratio continuously decreases from one at small impact angles to about 0.5 at normal impact. This demonstrates the high energy loss for soft wall material as a result of the strong deformation of the wall during the impact. The analysis of the velocity dependence of the restitution coefficient revealed a continuous decrease with increasing impact velocity and hence deformation of the wall.

A number of experimental studies on particle-wall collisions were also performed by Petrak and co-authors (Frank et al., 1993; Schade et al., 1996). In the initial studies a particle laden jet was directed towards an inclined plate of different material (Frank et al., 1993) and the particle velocity was measured using a special fibre optical probe. In the experiments glass beads with a diameter of 115 μm were used and impact angles of 10°, 30° and 45° were considered. Moreover, the influence of wall roughness was analysed using targets with different degree of roughness. The particle velocity before impact was varied between 4 and 13 m/s. The results for the restitution ratio (i.e. the measured ratio of the normal velocity component after impact to that before impact) are in contradiction to previous findings (e.g. Martin et al., 1991) since very low values are reported for small impact angle. Moreover, no clear trends are shown for the effect of wall roughness and too few results are presented in order to allow a detailed analysis of wall roughness effects. The main difficulty in the interpretation of the results is caused by the fact that not individual particle impacts are analysed, rather the behaviour of the jet and its declination by the wall is measured by the applied probing technique. Hence, the results are not very useful for deriving the required model constants.

Therefore, in a later study (Schade et al., 1996) a test facility was used which allows to analyse single particle impacts. Again glass beads with a mean diameter of about 110 μm were used and the effect of different target materials was studied. But still the rebound properties of the particles were obtained by statistical averaging and not for each individual event since again the fibre probe was used for velocity measurements. Therefore, the restitution ratios reported for small impact angles are doubtful since the values are below unity even for a rough wall. From the physical interpretation given by Sommerfeld et al. (1993), Sommerfeld and Huber (1995), it is obvious that the restitution ratio must be larger than unity for small impact angles and rough walls. Additionally, results on the friction coefficient are presented by Schade et al. (1996) showing a dependence on the impact velocity and the impingement angle. For impact angles between 5° and 60° a drastic decrease of the friction coefficient from about 1.5 to 0.2 is reported. In a study published earlier by Sommerfeld and Huber (1995) similar results on the coefficient of friction are presented.

In the studies by Shaffer et al. (1994) the collision of solid particles with the wall was analysed by particle tracking velocimetry. However, only a limited number of impact conditions were considered so that no correlations useful for modelling could be derived.

2. Test facility

For providing reliable data for the collision of particles with rough walls, measurements were conducted in a particle laden horizontal channel flow (Fig. 1). The channel height was 30 mm and the width 300 mm so that a two-dimensional flow was established. The length of the channel was 3 m which allowed for fully developed flow conditions at the end of the channel for particle sizes up to about 200 μm. The top and bottom walls of the channel were made of stainless steel plates, and the side walls were 3 mm thick glass plates. Other materials for the top and bottom walls (i.e. polished steel, Plexiglas and rubber) were also considered. This was accomplished by inserting plates of the respective material into the channel. At the end of the channel, a casing with a glass window was mounted for allowing optical access. The analysis of particle-wall collisions in a channel flow has the advantage that the impact occurs under realistic conditions and the particles may also rotate due to previous wall collisions.

For the visualisation of the particle trajectories the particle tracking velocimetry in the streak line mode was applied. A pulsed laser light sheet was produced by a 5 W Argon–Ion laser, a Bragg cell, and a set of cylindrical lenses. The light sheet was send along the centre of the channel through the window at the end wall of the channel. The Bragg cell was used as an acoustic optical deflector to pulse the light sheet at a pre-defined frequency and pulse length. This was achieved by a mono-stable multi-vibrator controlled by two 12 bit counters and a controlling logic unit. This electronic device was used to generate a square wave function to trigger a 40 MHz Bragg cell driver unit. With the help of this unit it was possible to switch the first order beam after the Bragg cell very precisely. The switch frequency and the pulse duration could be selected independently. The smallest pulse or pause time was 1 μs. This method of pulsing a continuously working laser has the advantage that the contrast of the light pulses and the efficiency of the light transmittance are very high, namely 70%.

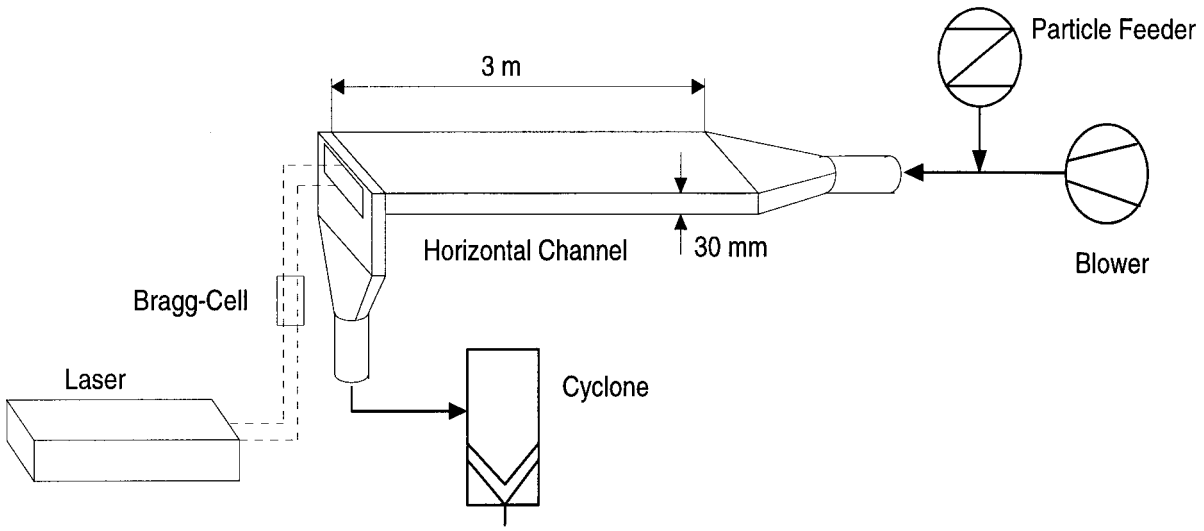

Fig. 1. Drawing of horizontal channel test facility together with the visualisation system.

The particle traces in the near wall region of the channel flow at a location 2.8 m downstream of the beginning of the channel were recorded by a CCD-Camera (Hitachi, Type KP-M1) which has a resolution of 736 × 581 pixels. The light intensity resolution of the CCD-camera was 8 bit which corresponds to grey levels between 0 and 255. A 55 mm Canon lens with an aperture opening of $f^{\#} = 1.1$ was used in connection with a 10 mm adapter ring to obtain a large magnification. A series of individual images of the particle traces were recorded on a video tape during the measurement period. In order to obtain the required statistical information several thousands of images were recorded. The processing of the images was performed off-line and fully automated using a PC AT-486, a frame grabber card (Matrox IP-8/AT) and a relays box which controlled the video recorder output.

The video recorder for storing and replaying the images of the particle trajectories was a Panasonic AG7330. This recorder possesses an interface for remote control with electronic signals. For this purpose a relays box was build which receives 8 bit words from the parallel port of the computer and then switches different functions of the video recorder. Since the analysis of the images takes about 4 s the video recorder was operated in the single-frame stepping mode. After the analysis of one frame an 8 bit code is written to the parallel port and a new frame of the video tape is displayed.

3. Image analysis

For the identification and validation of the particle traces and for the calculation of the change of particle velocity and trajectory angle during a wall collision, a processing software was developed which is described in the following section. The image analysis involves the following steps:

- grabbing of a frame from the video tape and digitisation,
- binarisation of image,
- identification of wall and particle streak lines,
- identification of streak lines belonging to a wall impact of one particle,
- determination of particle velocities and trajectory angles before and after impact,
- statistical treatment of data to obtain mean values as a function of impact angle.

For grabbing the frames, C-library functions were used that were supplied together with the frame grabber card. The contrast of the images was optimised at the beginning of the processing by properly adjusting gain and offset. A number of different approaches to enhance the image were tested, such as convolution filters, but a simple binarisation with a resolution of up to 256 grey levels was found to be fast and reliable. Since the brightness of the images was not strongly varying, the required threshold level for binarisation was kept constant for one set of experiments. The result of the binarisation is illustrated in Fig. 2, showing a typical image of the particle trajectories. The wall appears as a bright horizontal line at the upper bound of the frame. For finding the particle streak lines and the wall, the matrix of the pixels is scanned searching for bright objects. Only those objects having more than 10 pixels are identified as a streak line. Smaller objects are discarded since they may be the result of remaining noise or particle trajectories which are oblique to the plane of the light sheet. For each streak line, the

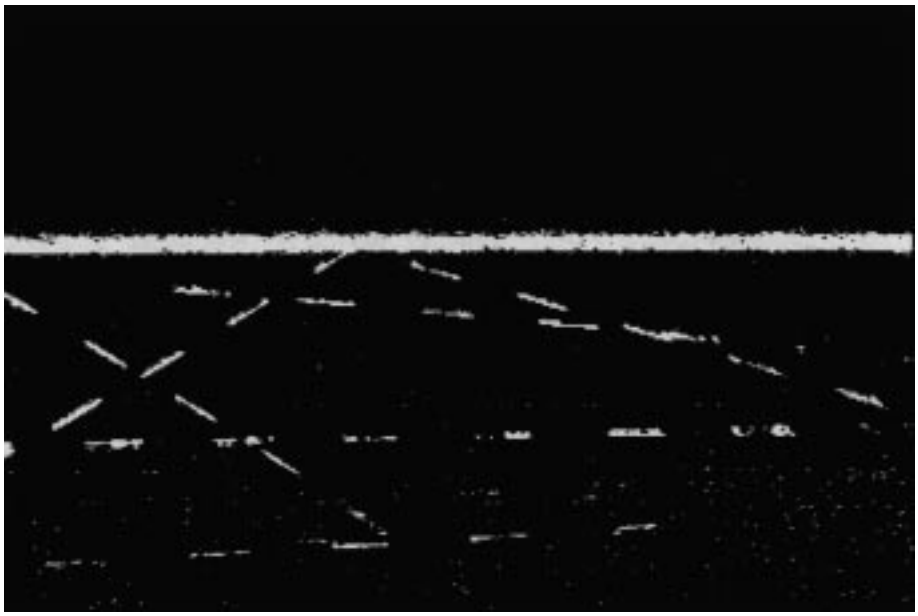

Fig. 2. Typical binarised image of particle trajectories.

number of pixels and their individual co-ordinates are determined. The slope, length, and width of the streak lines are determined by means of a linear regression. When the regression line intersects with the wall it is assumed that it belongs to a particle colliding with the wall or being rebound and its properties are stored. The next step in the processing algorithm is the identification of two streak lines before and after impact. For identifying these two wall-nearest pairs several criteria have to be met (Fig. 3):

- The slope of the regression lines of the two respective streak lines must be identical with certain pre-specified limits.
- The ratio of streak line length A to the streak line separation B must be within certain limits corresponding to the ratio of laser pulse duration to the time between pulses.
- The line through both respective streak lines before and after impact must intersect with the wall at about the same location.

Differences in the intersection location of the impact and rebound trajectory may result from the finite width of the streak lines and the occurrence of sliding collisions. The different threshold levels for the identification of a collision event were determined by a trial and error approach comparing the result of the processing algorithm with the video image. Due to the finite size of the image, additionally a so-called boundary region error has to be considered. In the regions D1 and D2 only particle trajectories with large impact or rebound angles may produce two streak lines on the image. Hence the statistics for the determination of mean collision properties will be biased with respect to a stronger weighing of large trajectory angles. In order to avoid this error no collision events are considered which have their point of impingement in the regions D1 and D2. The extension of these regions was adjusted according to the particle velocity and impact angle.

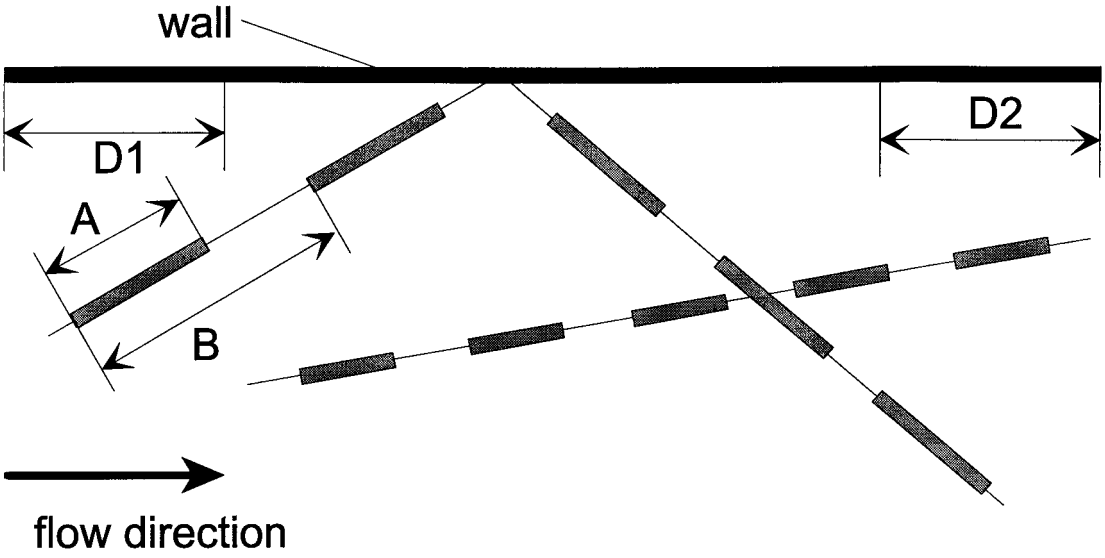

Fig. 3. Identification of streak lines belonging to the collision of one particle.

For evaluating the particle velocity components before and after impact the distances in x- and y-direction of the centres of two neighbouring streak lines are used and divided by the pulse separation time (Fig. 4). This approach was found to be more accurate than using the length of the streak lines and the pulse duration. Moreover, only two streak lines adjacent to the wall are considered, since especially for smaller particles the particle trajectories may become non-linear. A determination of the velocities from more than two streak lines may then

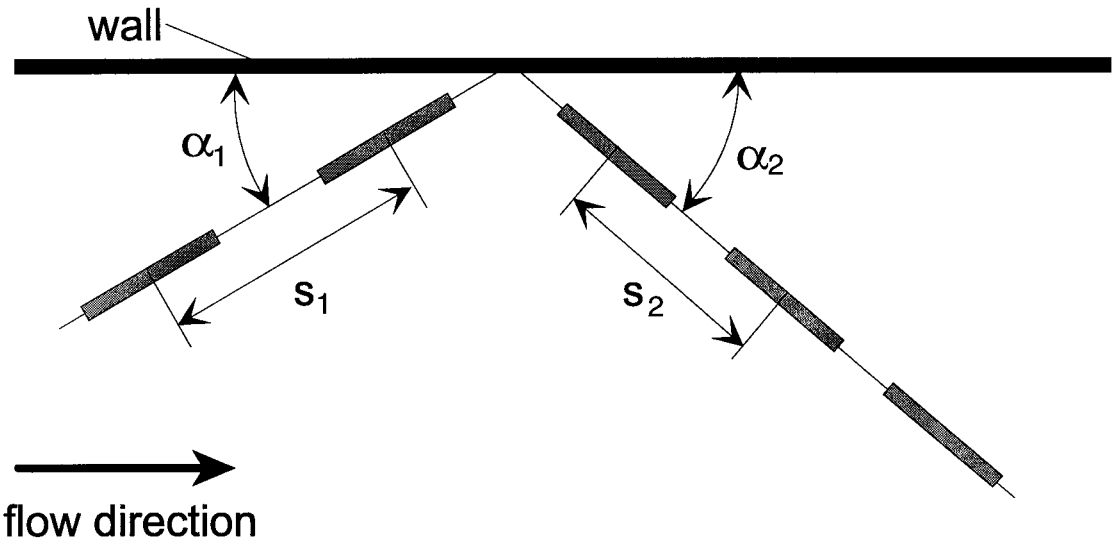

Fig. 4. Determination of velocities and impact and rebound angles.

result in considerable errors. Finally it is also ensured, that the absolute value of the particle velocity after rebound is smaller than the impact velocity.

The accuracy of the velocity determination depends on the spatial resolution of the streak lines (i.e. their separation) and the accuracy of the pulse frequency. The error in the pulse frequency was estimated using a digital oscilloscope and was found to be about 1%. For an image width of about 20 mm the spatial resolution is about 25 μm/pixel. The pulse frequency was adjusted to yield a streak line separation of about 2 mm. This results in an error for the determination of the streak line separation of about 1.3%. Hence, the error in the determination of the absolute particle velocity is about 1.7%.

For each particle-wall impact now the absolute velocity, the velocity components in x- and y-direction and the trajectory angle for impact and rebound are available. For deriving the mean values and the wall collision parameters such as restitution ratios and friction coefficients as a function of impact angle, between 1000 and 5000 events are considered.

4. Wall collision model and evaluation of collision parameters

With the light sheet method only collisions in one plane are detected. Hence, the momentum equations for the wall collision process in two-dimensional form may be used to evaluate the collision parameters. The solution of the momentum equations together with Coulombs law of friction yields a set of equations for a sliding and non-sliding collision process (Tsuji et al., 1987; Sommerfeld, 1992). The condition for a non-sliding collision is obtained in the following form:

$$\left| u_{p1} - \frac{D_p}{2}\omega_{p1} \right| \leq \frac{7}{2}\mu_0(1+e)v_{p1} \tag{1}$$

Here, the subscript 1 refers to the particle velocity components before impact, e is the coefficient of restitution relating the normal velocity component after the collision to that before the collision, μ_0 is the static coefficient of friction, and D_p is the particle diameter. Furthermore, u_p and v_p are the particle linear velocities parallel and normal to the wall, respectively, and ω_p is the angular velocity of the particle (Fig. 5). The particle linear and rotational velocities after rebound (subscript 2) are obtained from the momentum equations for the collision configuration shown in Fig. 5. For a *collision without sliding* one obtains:

$$u_{p2} = \frac{1}{7}\left(5u_{p1} + D_p\omega_{p1}\right)$$

$$v_{p2} = -ev_{p1}$$

$$\omega_{p2} = 2\frac{u_{p2}}{D_p} \tag{2}$$

The velocity components after a *sliding collision* are calculated by:

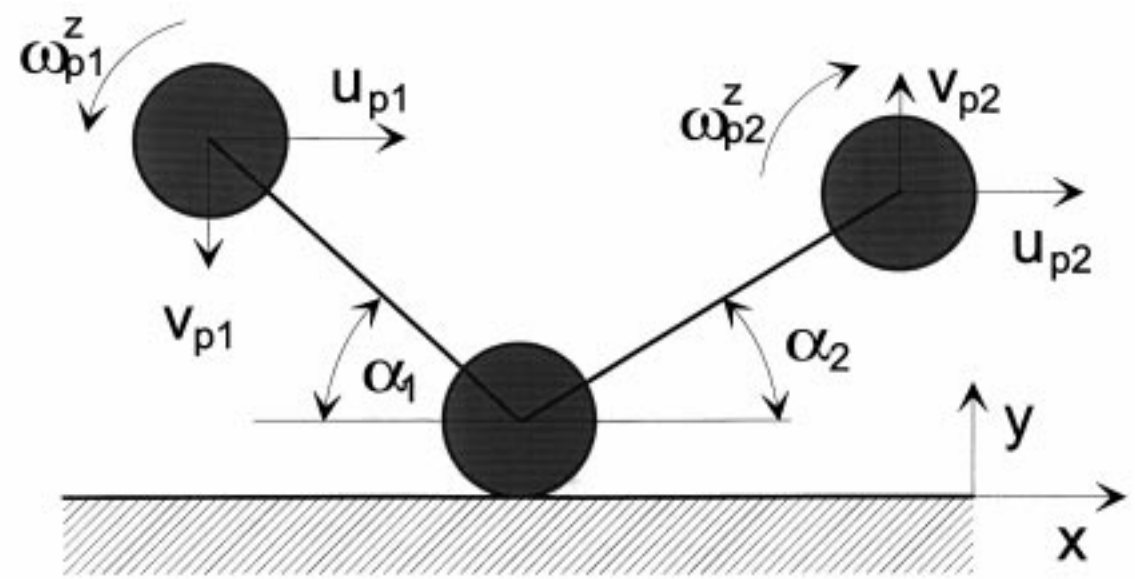

Fig. 5. Definition of velocities and angles before impact and after rebound.

$$u_{p2} = u_{p1} - \mu_d(1+e)\varepsilon_0 v_{p1}$$

$$v_{p2} = -e v_{p1}$$

$$\omega_{p2} = \omega_{p1} + 5\mu_d(1+e)\varepsilon_0 \frac{v_{p1}}{D_p} \tag{3}$$

In these equations, μ_d is the dynamic friction coefficient, and ε_0 indicates the direction of the relative velocity between particle surface and wall given by:

$$\varepsilon_0 = \mathrm{sign}\left(u_{p1} - \frac{D_p}{2}\omega_{p1}\right) \tag{4}$$

For simulating the wall roughness effect a stochastic approach was adopted (Sommerfeld, 1992, 1996; Sommerfeld et al., 1993) by assuming that the impact angle is composed of the particle trajectory angle α_1 and a stochastic contribution due to wall roughness:

$$\alpha_1' = \alpha_1 + \Delta\gamma\xi \tag{5}$$

From experiments (Sommerfeld and Huber, 1995) and numerical simulations it was found that the probability of the roughness angle may be approximated by a normal distribution function with a standard deviation of $\Delta\gamma$. Hence, ξ represents a Gaussian random variable with zero mean and a standard deviation of one. The value of $\Delta\gamma$ depends on the structure of the wall roughness and additionally on the particle size.

In order to determine the roughness angle distribution as a function of particle size, the wall material used in the channel facility was optically scanned with a resolution of 1 μm (Fig. 6).

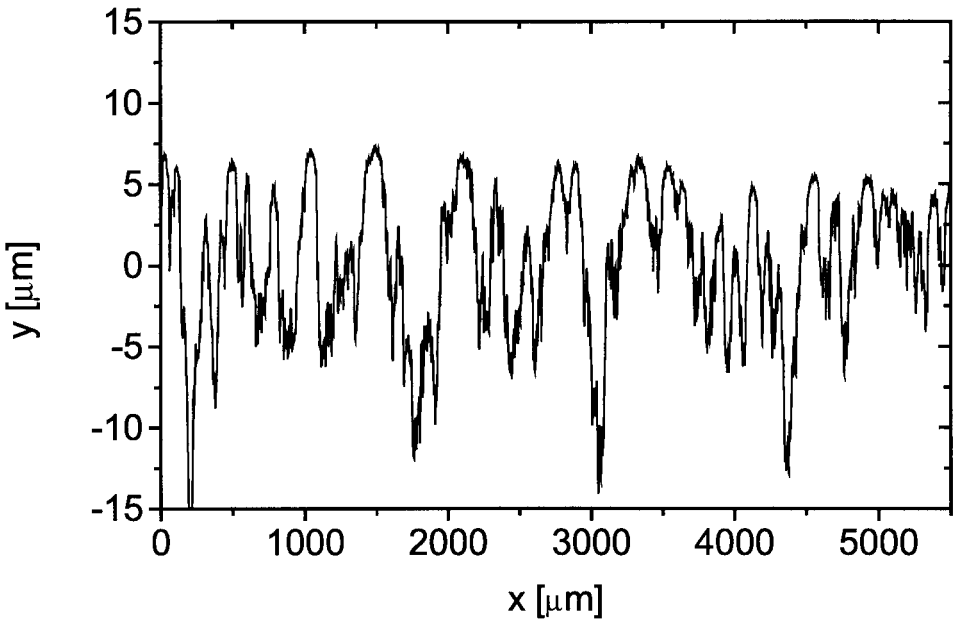

Fig. 6. Scanned profile of the wall roughness structure for a stainless steel plate (average roughness height according to DIN 4768 : 25 μm).

The average roughness height for the stainless steel wall was found to be 25 μm (according to DIN 4768). By sampling the roughness profile with different intervals and determining the inclination over this distance one can obtain a roughness angle distribution. The resulting distributions shown in Fig. 7(a) and (b) for a sampling distance of 20 and 100 μm, respectively, may be approximated by a normal distribution function, as assumed in the model. The resulting probability distribution function (PDF) is given by:

$$P(\Delta\gamma,\gamma) = \frac{1}{\sqrt{2\pi\Delta\gamma^2}}\exp\left(-\frac{\gamma^2}{2\Delta\gamma^2}\right) \tag{6}$$

From the distribution functions for the different sampling distances a mean value and a standard deviation (i.e. rms value) can be calculated (Fig. 8). The mean value of the roughness angle distribution is almost zero except for very small sampling distance. The standard deviation which is in some way correlated with the particle size (i.e. sampling distance) continuously decreases with increasing sampling distance. Hence, the roughness effect will be larger for smaller particles.

As demonstrated previously, there exists also a so-called shadow effect for small particle impact angles (Sommerfeld and Zivkovic, 1992; Sommerfeld, 1996; Schade and Hädrich, 1998) which implies that the particles may not hit the lee side of a roughness structure when the absolute value of the negative inclination angle $|\gamma_-|$ becomes larger than the impact angle (Fig. 9). This results in a higher probability for the particle to hit the luff side and a shift of the probability distribution function of the effective roughness angle towards positive values.

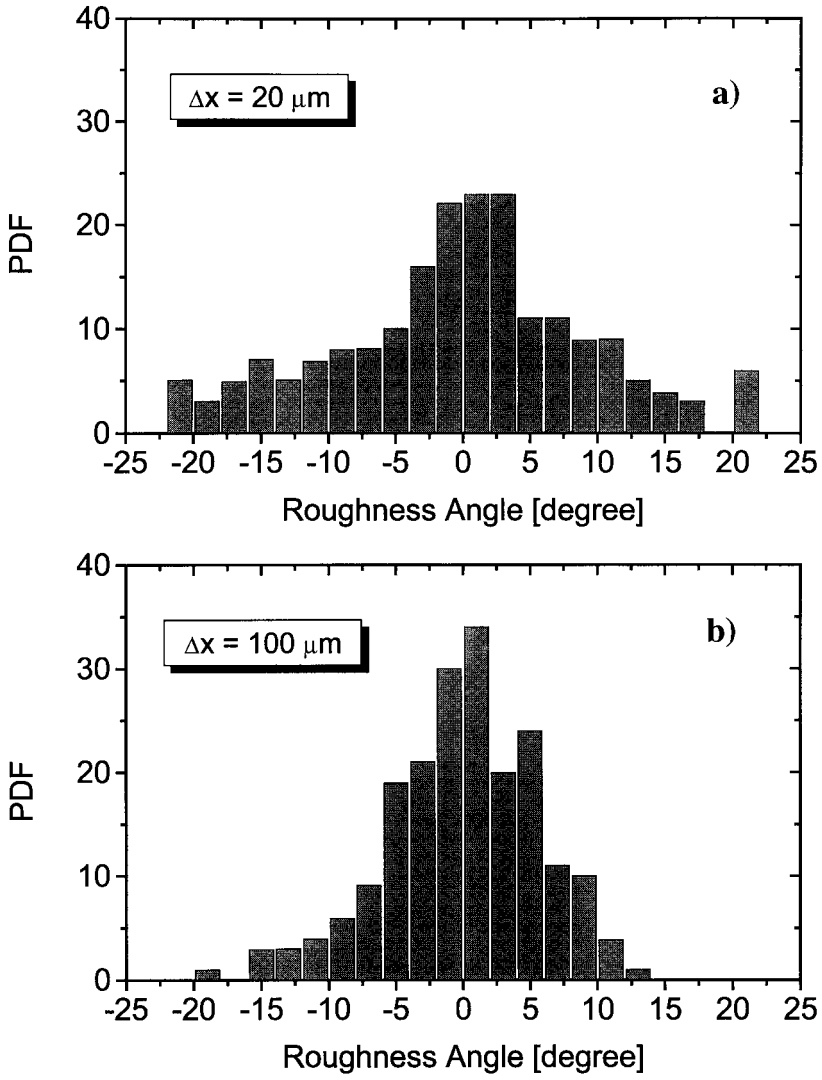

Fig. 7. Probability distribution functions of the roughness angle for different sampling distance, (a) 20 μm, (b) 100 μm.

Therefore, there exists a mean roughness angle which depends on particle size and the impact angle. For a given combination of α_1 and γ the following three regimes of the effective roughness angle distribution function may be identified:

1. The particle cannot hit a roughness structure with $|\gamma_-| > \alpha_1$ whereby the probability becomes zero:

$$f(\alpha_1,\gamma) = 0 \tag{7}$$

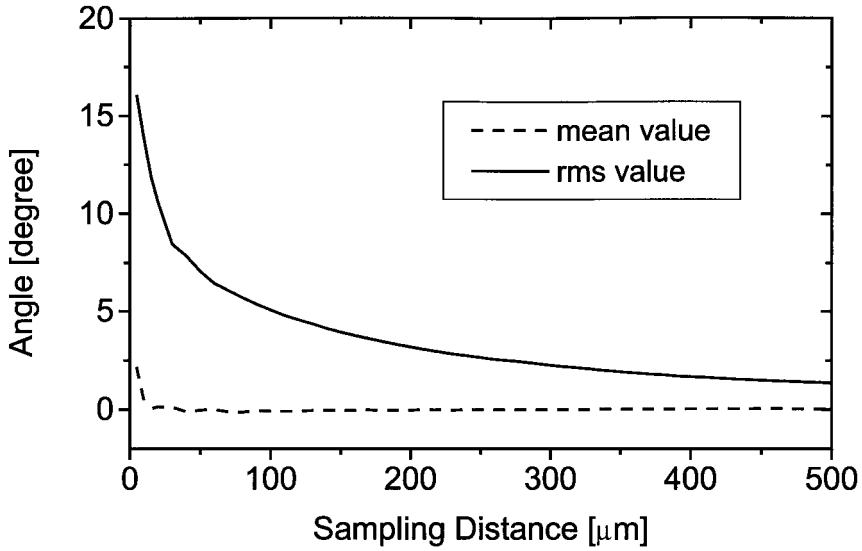

Fig. 8. Mean value and rms value of the roughness angle distribution functions in dependence on the sampling distance.

2. The probability to hit a roughness structure with a negative inclination in the interval $0<|\gamma_-|<\alpha_1$ is smaller than that to hit a horizontal wall by the factor:

$$f(\alpha_1,\gamma) = \frac{\sin(\alpha_1 + \gamma_-)}{\sin \alpha_1} \tag{8}$$

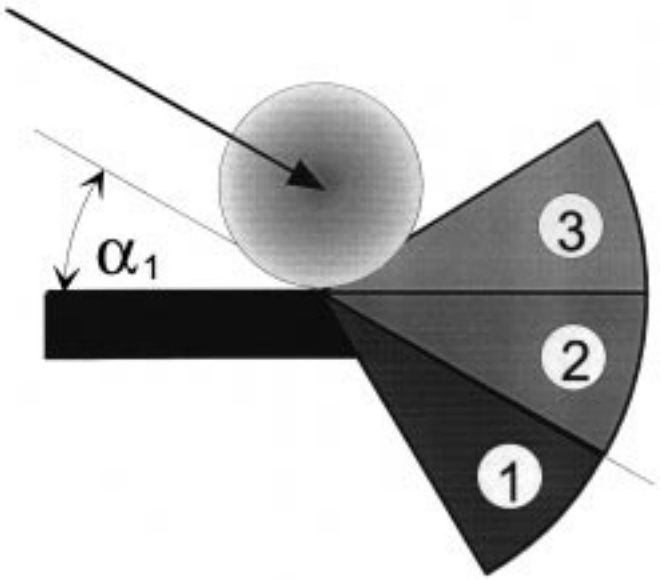

Fig. 9. Illustration of shadow effect due to wall roughness for small impact angles.

3. The probability to hit a positive inclined wall roughness structure (i.e. $\gamma = \gamma_+ > 0$) is higher than that to hit a horizontal wall by the factor:

$$f(\alpha_1,\gamma) = \frac{\sin(\alpha_1 + \gamma_+)}{\sin \alpha_1} \tag{9}$$

The effective distribution function of the wall roughness inclination seen by the particle is finally obtained in the following form:

$$P_{\text{eff}}(\alpha_1,\Delta\gamma,\gamma) = P(\Delta\gamma,\gamma) f(\alpha_1,\gamma) = \frac{1}{\sqrt{2\pi\Delta\gamma^2}} \exp\left(- \frac{\gamma^2}{2\Delta\gamma^2} \right) \frac{\sin(\alpha_1 + \gamma)}{\sin \alpha_1} \tag{10}$$

The effective mean roughness angle may now be calculated by integrating the distribution function from $\gamma = \alpha_1$ to $\gamma \to \infty$.

$$\bar{\gamma}_{\text{eff}}(\Delta\gamma,\alpha_1) = \int_{\alpha_1}^{\infty} \gamma P_{\text{eff}}(\alpha_1,\Delta\gamma,\gamma)\, \mathrm{d}\gamma \tag{11}$$

The effective roughness angle distribution functions are plotted in Fig. 10 for different impact angles together with the original normal distribution function and the distributions sampled in the model calculations. It is obvious that the shadow effect reduces with increasing impact angle and as a result, the distribution function of the effective roughness angle approaches the shape of the normal distribution function. The effective roughness angle distributions obtained from the model calculations agree reasonably well with the result obtained from Eq. (10) but slightly under-predicts the mean roughness angle, $\bar{\gamma}_{\text{eff}}$, and also the effective standard deviation $\Delta\bar{\gamma}_{\text{eff}}$ (Fig. 11). The procedure to account for the shadow effect in the model is as follows:

- The roughness angle is sampled from the normal distribution function (Eq. (6)).
- If a negative roughness angle with an absolute value being larger than α_1 is sampled, an unphysical collision results, namely the particle would come from behind the wall and hence a new value is sampled for γ.

With this method, the resulting distribution function is automatically shifted towards positive values (Fig. 10).

In the following, the procedures to evaluate the parameters relevant for the wall collision model are described. The change of particle velocity during a wall impact is expressed with the velocity ratios (i.e. restitution ratio) normal and parallel to the wall:

$$R_{\text{N}} = \frac{v_{\text{p2}}}{v_{\text{p1}}}, \qquad R_{\text{P}} = \frac{u_{\text{p2}}}{u_{\text{p1}}} \tag{12}$$

As a result of wall roughness the normal velocity ratio may become larger than one for small impact angles. In the equations for calculating the velocity change by a wall impact (Eqs. (1)–(3)) however a restitution coefficient e is needed which is only related to the loss of momentum as a result of the deformation of wall and particle during the impact which depends on the material properties of particle and wall and the impact angle. Hence, this coefficient should not include wall roughness effects. For the determination of the mean restitution coefficient as a

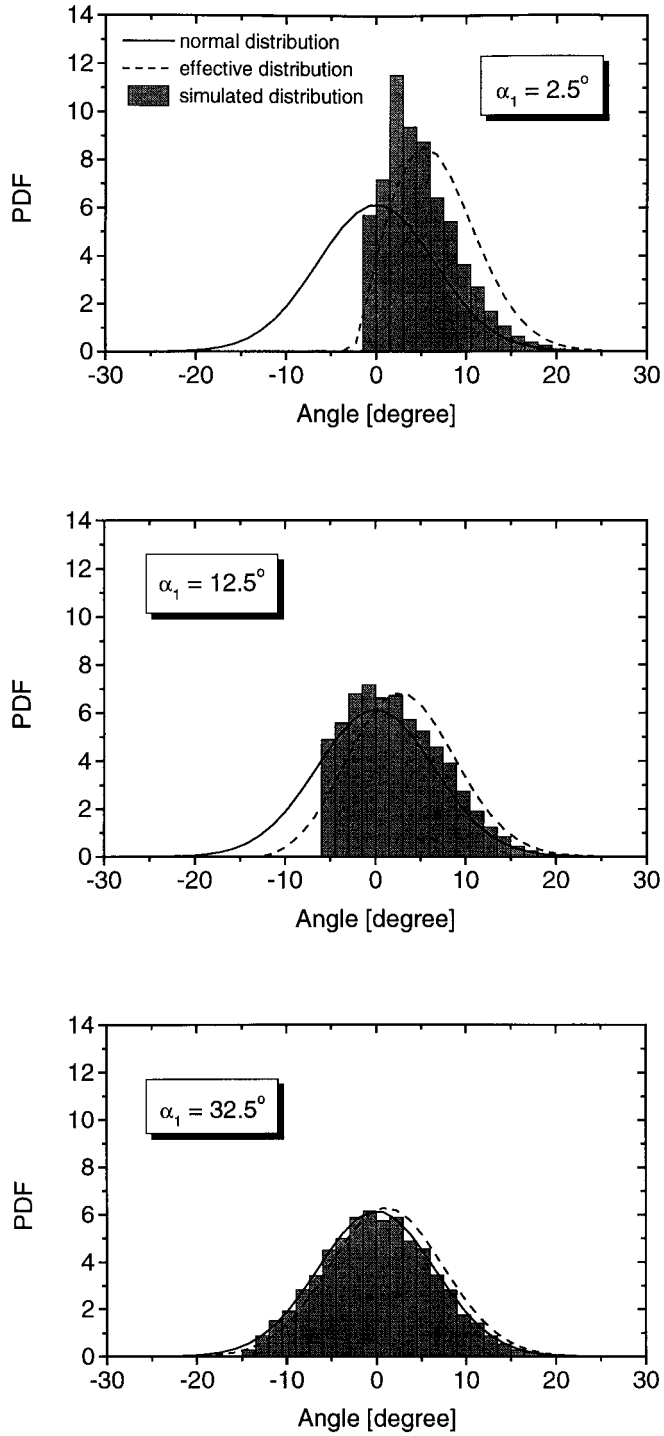

Fig. 10. Modification of roughness angle distribution due to the shadow effect for three different impact angles ($\Delta\gamma = 6.5°$).

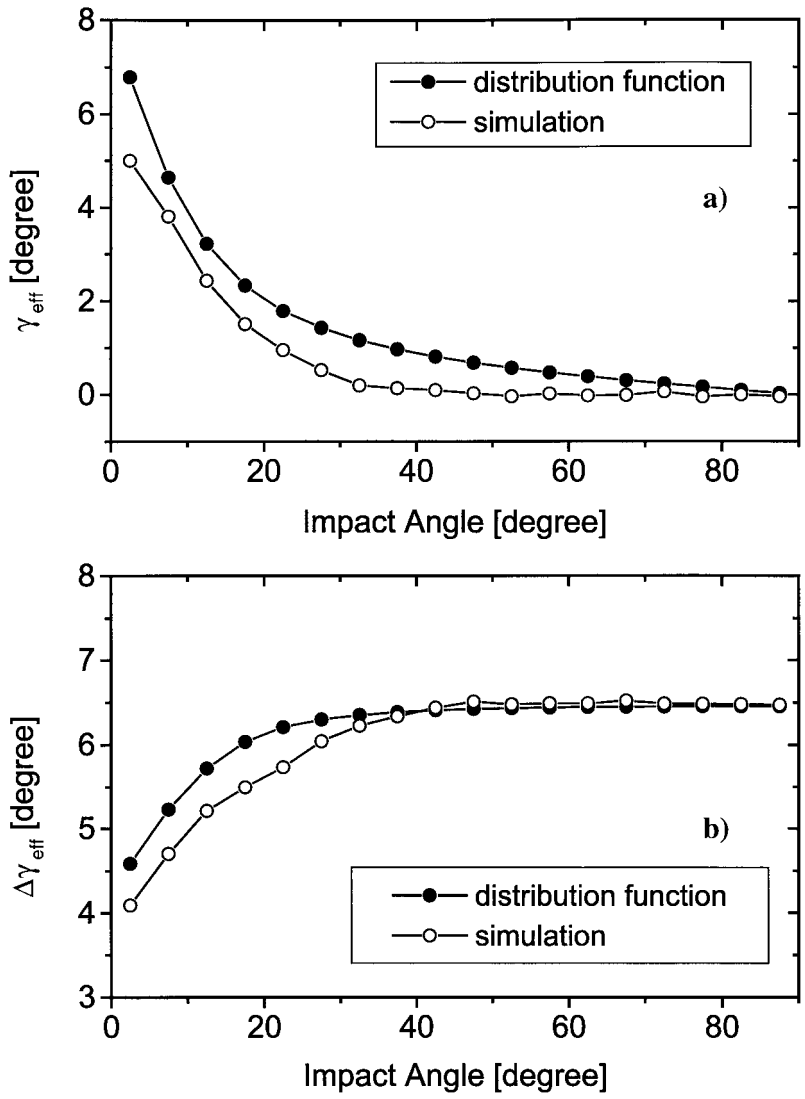

Fig. 11. Variation of effective mean roughness angle (a) and the effective standard deviation (b) with impact angle, comparison of the result obtained from the effective distribution function (10) and the model simulations ($\Delta\gamma = 6.5°$).

function of impact angle, trigonometric relations may be used and one obtains:

$$e(\alpha_1) = \frac{\sin(\alpha_2 - \bar{\gamma}_{\text{eff}})|u_{\text{p2}}|}{\sin(\alpha_1 + \bar{\gamma}_{\text{eff}})|u_{\text{p1}}|} \tag{13}$$

The evaluation of the mean values of $e(\alpha_1)$ requires in addition to the collision data obtained from the PTV the knowledge of $\bar{\gamma}_{\text{eff}}$ and hence the standard deviation of the roughness angle distribution $\Delta\gamma$ (see Eqs. (10) and (11)). This value depends on the roughness structure, the

material of particle and wall and the particle size. All these parameters determine the degree of deformation during the impact.

In order to correlate the standard deviation of the roughness angle distribution with the particle size the following approach was adopted. Since the restitution coefficient e is associated with the momentum loss during the impact and hence with the deformation of particle and wall it may be expected that if α_1 approaches zero the restitution coefficient should approach unity. Therefore, one can use Eqs. (11) and (13) to determine the standard deviation $\Delta\gamma$. The integration of the effective roughness angle distribution (10) to obtain the mean roughness angle $\bar{\gamma}_{\text{eff}}$ was done numerically, since an analytic solution does not exist. By considering the data collected for the smallest impact angle (i.e. in this case $\alpha_1 = 2.5^\circ$) and varying $\Delta\gamma$ from one degree to some upper limit, it is possible to obtain the intersection of this curve with $e = 1$ as illustrated in Fig. 12 for different particles and wall materials. The $\Delta\gamma$-value at this intersection is relevant for the considered combination of particle and wall. It is obvious from Fig. 12 that $\Delta\gamma$ decreases with increasing particle size and that some roughness effect is also found for small particles and a polished steel wall. The values of $\Delta\gamma$ obtained from Fig. 12 can now be used to calculate the restitution coefficient as a function of impact angle using Eqs. (11) and (13) and the experimental data, i.e. the velocity ratio R_{P}. The results will be discussed in the next section.

Finally, the coefficient of friction may be determined from the equations describing a sliding collision. From Eq. (2) it follows that:

$$D_{\text{p}}\omega_{\text{p1}} = 7u_{\text{p2}} - 5u_{\text{p1}} \tag{14}$$

Inserting the condition for distinguishing a sliding and non-sliding collision (Eq. (1)) the particle rotation and the diameter are eliminated and one finally obtains for the coefficient of friction the following equation:

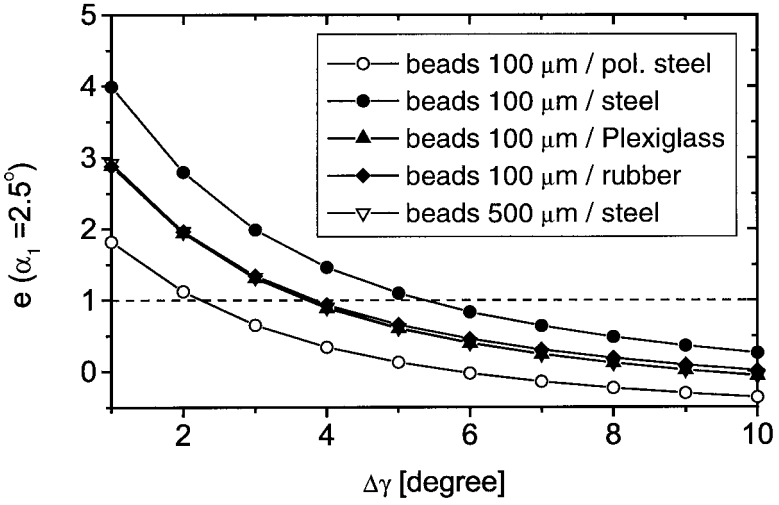

Fig. 12. Restitution coefficient as a function of the standard deviation of the roughness angle distribution.

$$\mu = \frac{|u_{p1} - u_{p2}|}{(1+e)v_{p1}} \tag{15}$$

With this approach no difference is made between the static and dynamic coefficient of friction.

5. Experimental results

For allowing a detailed analysis of the effects of particle size, particle shape, wall material, and wall roughness on particle-wall collisions, experiments were conducted for different combinations of particle and wall material as summarised in Table 1. In addition, some characteristic parameters for the wall collision model are summarised in Table 1, which will be discussed later. The particles used were spherical glass beads and irregular shaped quartz particles. The conveying velocity was kept constant with a value of about 15 m/s. The average impact velocity of the particles is of course lower since they lag behind the flow due to their inertia. The average absolute value of the impact velocities are also given in Table 1. The particle concentration was very low in order to allow the application of particle tracking velocimetry.

For illustrating the particle rebound behaviour for different wall materials, scatter plots of the rebound angle versus the impact angle are shown in Fig. 13, each for about 1000 individual events. Furthermore, the resulting mean values are included in the figures, which are averaged over an impact angle interval of 5°. Since the experiments were conducted in a narrow channel, the range of observed impact angles is relatively low, i.e. up to about 40°. For a polished steel wall and the 500 μm particles the data are scattered in a relatively narrow band close to the line of equal angles with a slightly higher probability of smaller rebound angles (Fig. 13(a)). Comparing this result with that obtained for a rough stainless steel wall reveals that wall roughness causes a much broader scattering of the data (Fig. 13(b)) and for small impact angles the mean rebound angle becomes larger than the impact angle. This effect is more pronounced for the 100 μm particles (Fig. 13(c)), since roughness is of greater importance for smaller ratios of the particle size to a characteristic dimension of the roughness (Sommerfeld,

Table 1
Summary of experimental conditions and parameters for the wall collision model[a]

Particles	Wall material	$U_{p1}(u'_{p1})$ (m/s)	$U_{p2}(u'_{p2})$ (m/s)	e_h	α_e (degree)	μ_0	μ_h	α_μ (degree)	$\Delta\gamma$ (degree)
Glass 100 μm	Steel polished	12.82 (1.63)	11.52 (1.81)	0.9	22	0.4	0.15	20	2.3
Glass 100 μm	Steel	13.32 (2.50)	11.34 (2.21)	0.7	22	0.5	0.15	20	5.3 (6.5)
Glass 100 μm	Plexiglass	9.75 (1.54)	8.33 (1.60)	0.73	18	0.4	0.15	27	3.8
Glass 100 μm	Rubber	11.31 (1.92)	9.16 (2.08)	0.5	18	0.8	0.02	35	3.8 (4.0)
Glass 500 μm	Steel polished	5.56 (1.01)	4.93 (1.02)	0.75	15	0.35	0.1	25	0.0
Glass 500 μm	Steel	5.91 (1.16)	5.15 (1.17)	0.7	22	0.4	0.15	20	3.8
Quartz 100 μm	Steel polished	16.04 (2.58)	13.37 (2.74)	0.55	27	–	–	–	2.6
Quartz 100 μm	Steel	15.02 (2.64)	12.05 (2.54)	–	–	–	–	–	3.7
Quartz 100 μm	Rubber	14.12 (2.76)	10.86 (2.82)	0.4	27	–	–	–	2.9

[a] Empty cells indicate that no data could be defined.

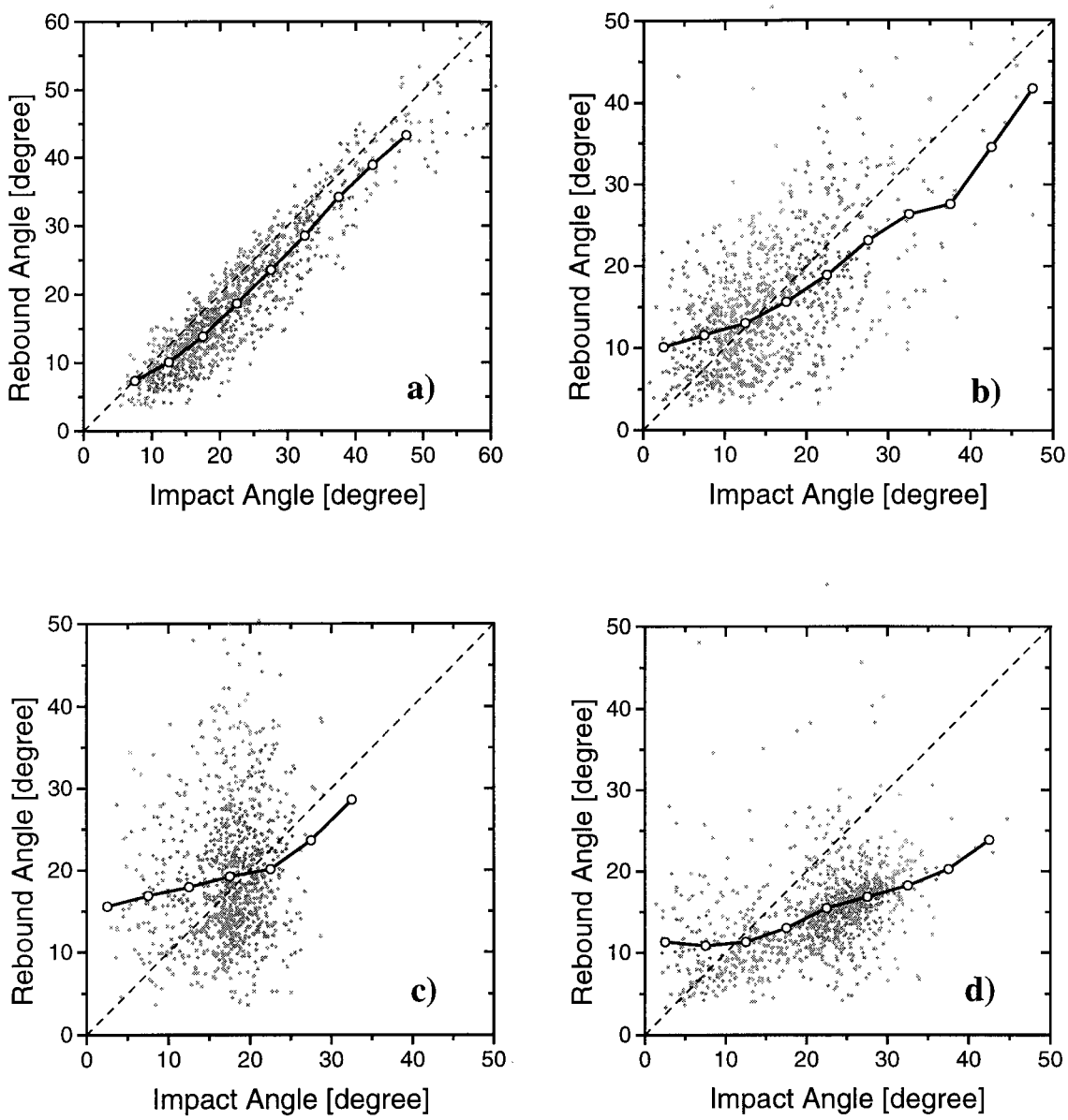

Fig. 13. Scatter plots of rebound angle versus impact angle for about 1000 events and measured averaged correlation between rebound angle and impact angle (closed line with symbols), (a) polished stainless steel wall and 500 μm particles, (b) stainless steel wall and 500 μm particles, (c) stainless steel wall and 100 μm particles and (d) rubber wall and 100μm particles.

1992). For a rubber wall the particle-wall impact is characterised by large elastic deformations. This results for larger impact angles in a stronger momentum loss whereby the rebound angles become much smaller than the impact angles (Fig. 13(d)). For small impact angles also a roughness effect is observed.

In most cases the rebound angle is larger than the impact angle up to a certain value. This is the so-called shadow effect which has been described above and results in an increase of the velocity component normal to the wall, as illustrated in Fig. 14 for the 100 μm particles and different wall materials. Even for the polished and the Plexiglas wall this effect is observed, which may be caused by slight non-sphericity of the particles (Tsuji et al., 1985) and probably some remaining wavy structures on the wall. The velocity ratio normal to the wall approaches almost constant values for large impact angles depending on the wall material. For the hard wall material the asymptotic values are between 0.75 and 0.8 and for the soft wall (i.e. rubber gum) which allows for a strong elastic deformation the velocity ratio approaches a much lower value of only 0.5. The difference of the asymptotic normal velocity ratio between polished steel and untreated steel is associated with a more local deformation of particle and wall due to the roughness. The restitution coefficient determined according to the procedure described above, shows a similar dependence on the impact angle as the ratio of the normal velocity components (Fig. 15). The curves for the different conditions show a decrease from one at $\alpha_1 = 0^\circ$ to an asymptotic value at an impact angle of α_e . With further increasing impact angle the restitution coefficient is almost constant. These asymptotic values are clearly correlated with the wall material and are summarised in Table 1. For a hard wall material (polished steel) the value is about 0.85 and for the soft wall (rubber) only 0.55. The asymptotic value for the Plexiglas wall is about 0.72, i.e. between the result for the hard and soft material.

The mean value of the friction coefficient plotted versus the impact angle determined according to Eq. (15) is shown in Fig. 16 again for the 100 μm particles. Except for the polished steel wall the friction coefficients have very high values for small impact angles, and decrease with increasing impact angle. For the steel walls and the Plexiglas wall the friction coefficient approaches a limiting value of about 0.15 for large impact angles. For the rubber

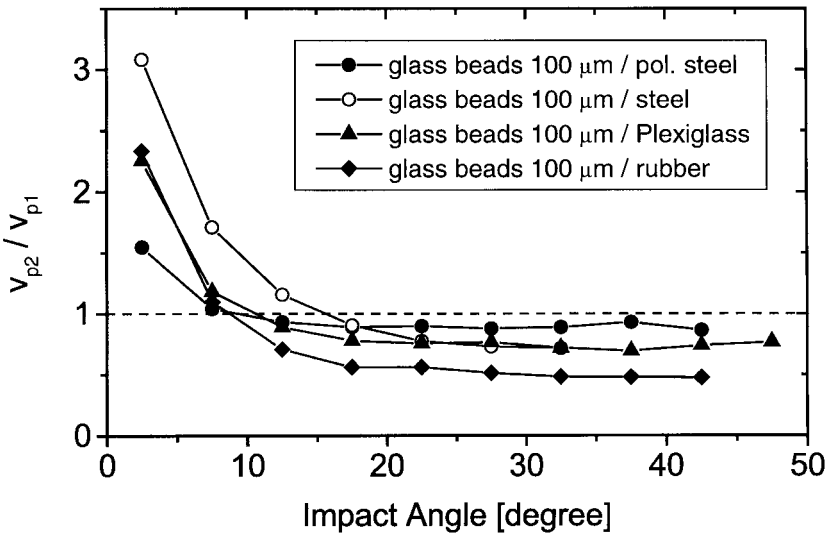

Fig. 14. Measured dependence of the velocity ratio for the component normal to the wall on the impact angle for different wall material and 100 μm glass beads.

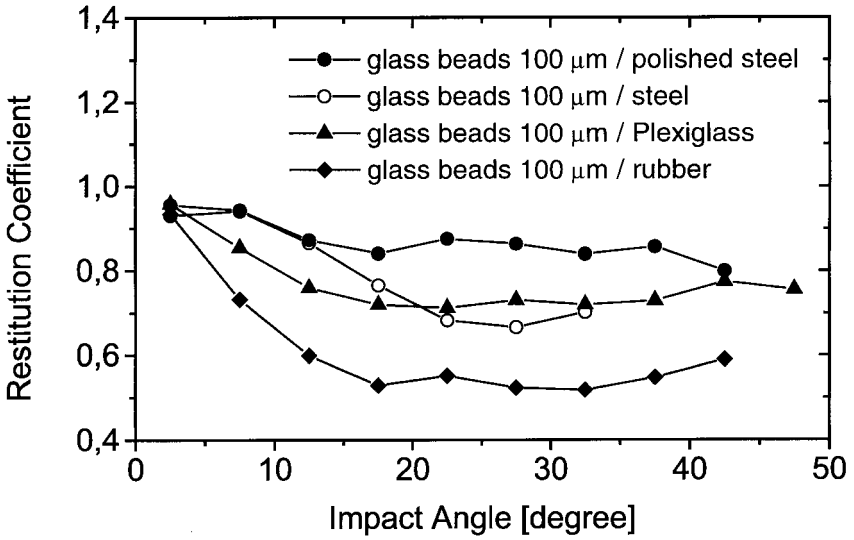

Fig. 15. Dependence of the restitution coefficient on the impact angle for different wall material and 100 μm glass beads, calculated using Eq. (13).

wall the asymptotic value comes close to zero. These asymptotic values are also summarised in Table 1 for the different cases, since they are relevant for the model.

The influence of particle size and shape is discussed for the polished stainless steel wall (Fig. 17(a)). The plot of the restitution coefficient reveals that the large glass beads cause a much stronger deformation during the impact compared to the smaller beads, although their impact velocity is lower (see Table 1). This is a result of the much higher particle mass. The limiting values for large impact angles are about 0.7 for the 500 μm and 0.85 for the 100 μm glass beads. For the non-spherical quartz particles the limiting value of the restitution coefficient is considerably lower than for the glass beads which is a result of the local strong deformation. In the case of the untreated stainless steel wall (Fig. 17(b)) the dependence of the restitution coefficient on the impact angle for small and large glass beads is quite similar for the range of impact angles considered and a limiting value of about 0.7 is approached for large impact angles. For the quartz particle an almost linear decrease of the restitution coefficient with increasing impact angle is observed. This is associated with a stronger local deformation of wall and particle as a result of the irregular shape of the particles and the resulting higher momentum loss.

This effect is also obvious from the ratio of the normal velocity component for the different particles shown in Fig. 18. At smaller impact angles the curve for quartz particles is very similar to that of the 500 μm spherical glass beads, but for larger impact angles the velocity ratio becomes considerable smaller than for the glass beads. From Fig. 18 it is also obvious that the wall roughness effect is more important for the smaller glass beads than for the larger ones. At an impact angle of 2.5° the normal velocity ratio has a value of 3.1 for the 100 μm particles and 2.2 for the 500 μm particles, respectively. The velocity ratio is larger than one up to an impact angle of about 11° and 16° for the large and small particles, respectively.

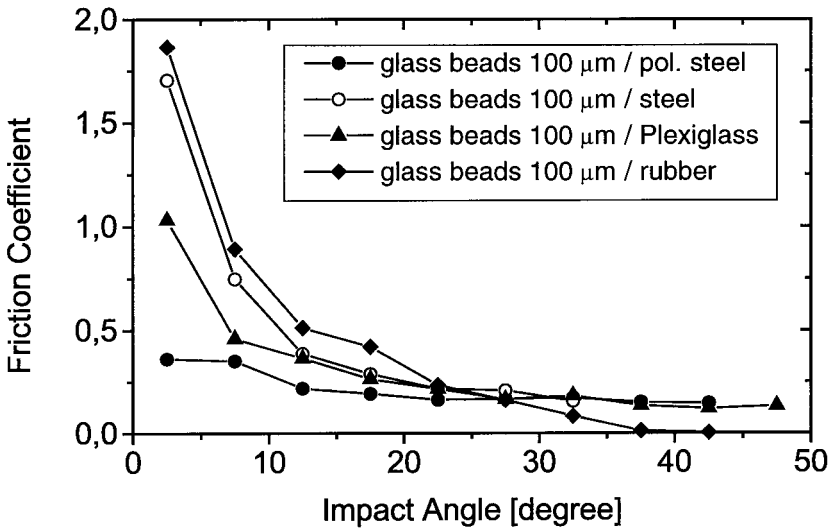

Fig. 16. Measured friction coefficient (i.e. calculated according to Eq. (15)) as a function of impact angle for different wall material and 100 μm glass beads.

The friction coefficient as a function of impact angle is also strongly dependent on particle size and particle shape and the degree of wall roughness. For the spherical glass beads (Fig. 19(a)) the friction coefficient approaches about the same value at large impact angles. At small impact angles the friction coefficient is considerably larger for the small particles which is again caused by wall roughness. The asymptotic value of the friction coefficient for the quartz particles is considerably larger than for the glass beads. Due to the irregular shape of the particles it is expected that edges of the particle will produce scratches and groves on the wall, resulting in relatively high values of the friction coefficient. Since for the stainless steel wall also roughness will alter the friction coefficient the above argument may be supported by results obtained for the polished steel wall (Fig. 19(b)). Also for this case the friction coefficient for the quartz particles is larger than for the glass beads and slightly lower than the friction coefficient for quartz particles colliding with a stainless steel wall (Fig. 19(a)). This difference is the contribution due to wall roughness.

6. Model calculations

For further refining and validating the wall collision model introduced by Sommerfeld (1992), simulations were performed for the different experimental conditions. For each condition the impact angle was varied in the range between 0° and 90°. The mean absolute impact velocity was specified according to the measured values (see Table 1). Statistical variations of the impact velocity were accounted for by sampling the instantaneous absolute velocity from a Gaussian distribution function with the measured rms value. No experimental data were however available on the angular velocity of the particles at impact. Therefore, the mean and rms values were selected by taking into account the particle size and the fact that the

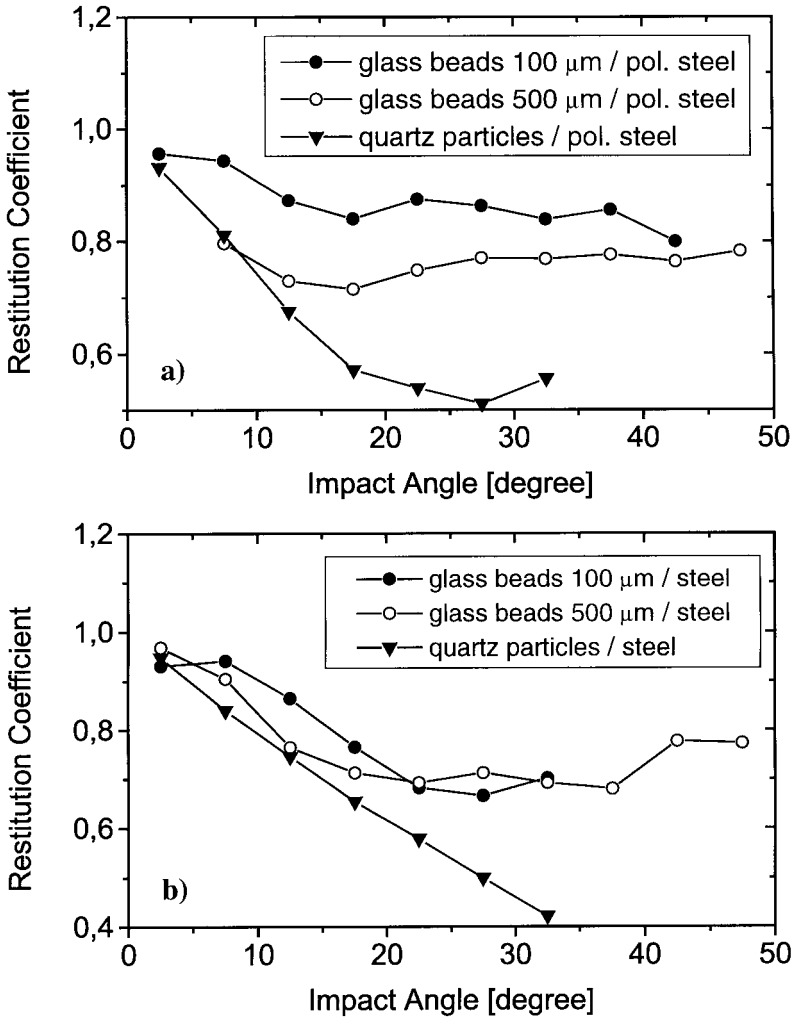

Fig. 17. Dependence of the restitution coefficient on the impact angle for different particles and a polished steel wall (a) and a stainless steel wall and (b), calculated using Eq. (13).

particles mainly will come from the opposite wall, resulting in a negative angular velocity. The maximum angular velocity just after rebound may be estimated using Eq. (2). The influence of the assumed angular velocity on the rebound velocities was however found to be not very strong for impact angles up to 40° as will be discussed below. For each impact angle 40.000 wall collisions were simulated by randomly sampling the instantaneous impact angle according to the procedure described above in order to account for wall roughness. Since the roughness effect is slightly under-predicted by the model (see Fig. 11), a larger value for $\Delta\gamma$ than obtained from the measurements (see Fig. 12) was used in some of the model calculations. This value is given in Table 1 in brackets. The angular and linear velocity components after rebound were calculated by solving Eqs. (1)–(3). The restitution coefficient as a function of instantaneous

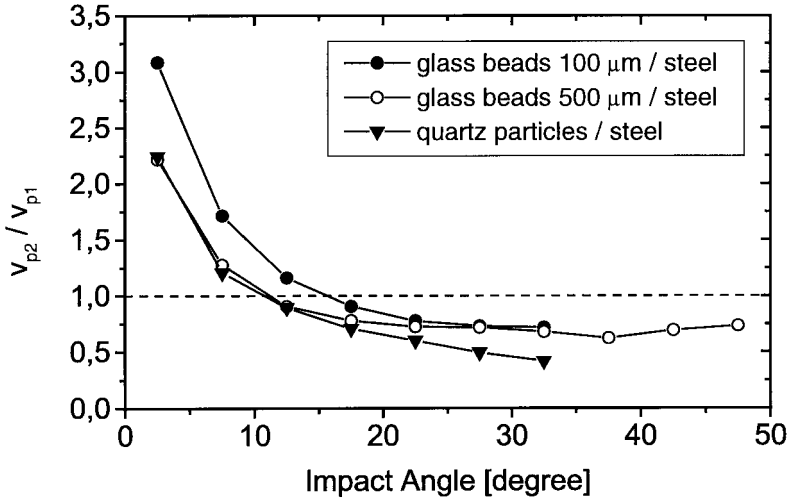

Fig. 18. Measured dependence of the velocity ratio for the component normal to the wall on the impact angle for the untreated stainless steel wall and different particles.

impact angle was approximated by a linear decrease from 1 at zero impact angle to e_n at an impact angle of α_e and a constant value of e_n for $\alpha_1 > \alpha_e$ as illustrated in Fig. 20(a). Since also the friction coefficient is affected by wall roughness, as demonstrated in Fig. 16, a similar segmented fit was assumed in the simulations as shown in Fig. 20(b). All the characteristic values assumed for the simulations are summarised in Table 1.

First the collision of 500 μm glass beads with the stainless steel wall is considered. In Fig. 21 the simulated probability distribution of the rebound angle for different impact angles is compared with the measurements. The effect of wall roughness results in broad distributions of the rebound angle as discussed above. The simulations are in reasonable agreement with the measurements for the considered impact angles. However, at small impact angles (i.e. for $\alpha_1 = 5^\circ$ and 15°) the predicted probability of small rebound angles (i.e. $\alpha_2 < 5^\circ$) is considerably higher as observed in the experiment.

The simulated mean values (i.e. friction coefficient, normal velocity ratio and parallel velocity ratio) as a function of impact angle are compared with the measurements for the 100 μm particles colliding with the stainless steel wall in Fig. 22. The agreement is reasonably well for all these values. Only the velocity ratio v_{p2}/v_{p1} is over-predicted for an impact angle of 2.5°, which indicates that the wall roughness effect is overestimated for small impact angles.

In order to demonstrate the importance of the presumed dependence of the friction coefficient on the impact angle for simulating correct rebound values, calculations with a constant friction coefficient of 0.15 and 0.5 are compared with the variable friction coefficient as a function of impact angle (Fig. 23). For low values of the impact angle the considered small value of the friction coefficient (i.e. $\mu = 0.15$) results in an underestimation of the effective friction coefficient up to an impact angle of about 30° (Fig. 23(a)). Hence, the velocity ratio parallel to the wall is overestimated (Fig. 23(b)). On the other hand, the higher value of the prescribed friction coefficient results in a good agreement with the simulations for very small impact angles and impact angles larger than about 55°. In the intermediate range the

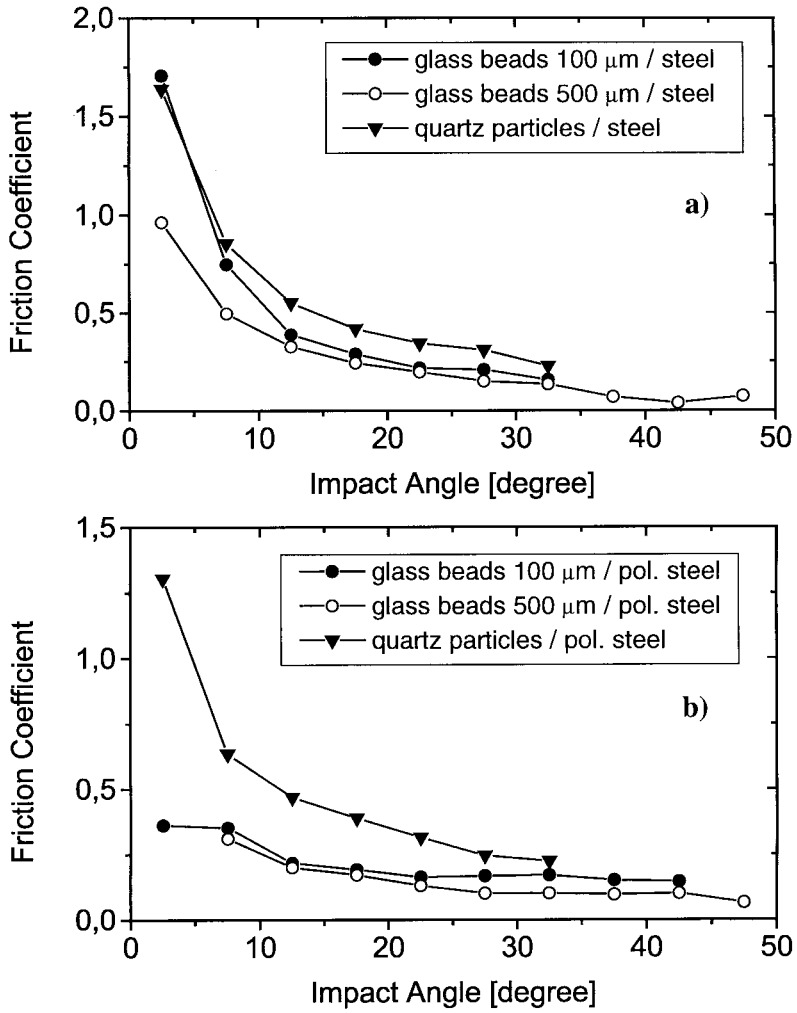

Fig. 19. Friction coefficient as a function of impact angle for different particles, (a) untreated stainless steel wall and (b) polished stainless steel wall.

effective friction coefficient is overestimated and as a consequence the velocity ratio parallel to the wall is underestimated. Hence, the best choice is a segmented fit of the prescribed friction coefficient, as shown in Fig. 20 with the parameters given in Table 1. The coincidence of the simulations with the different assumptions of the friction coefficient for impact angles larger than 60° is associated with the fact that at larger impact angles a collision without sliding occurs where the rebound properties are independent of the friction coefficient.

The effect of particle rotation on the wall collision process is analysed for 100 μm glass beads colliding with the polished steel wall by comparing results for negative and positive angular mean velocity of $\pm$30.000 1/s (Fig. 24) and a rms value of 10.000 1/s. It is obvious that the ratio of the normal velocity component is unaffected by the angular velocity in the entire range of impact angles (i.e. from 0 to 90°). However, the velocity ratio of the horizontal

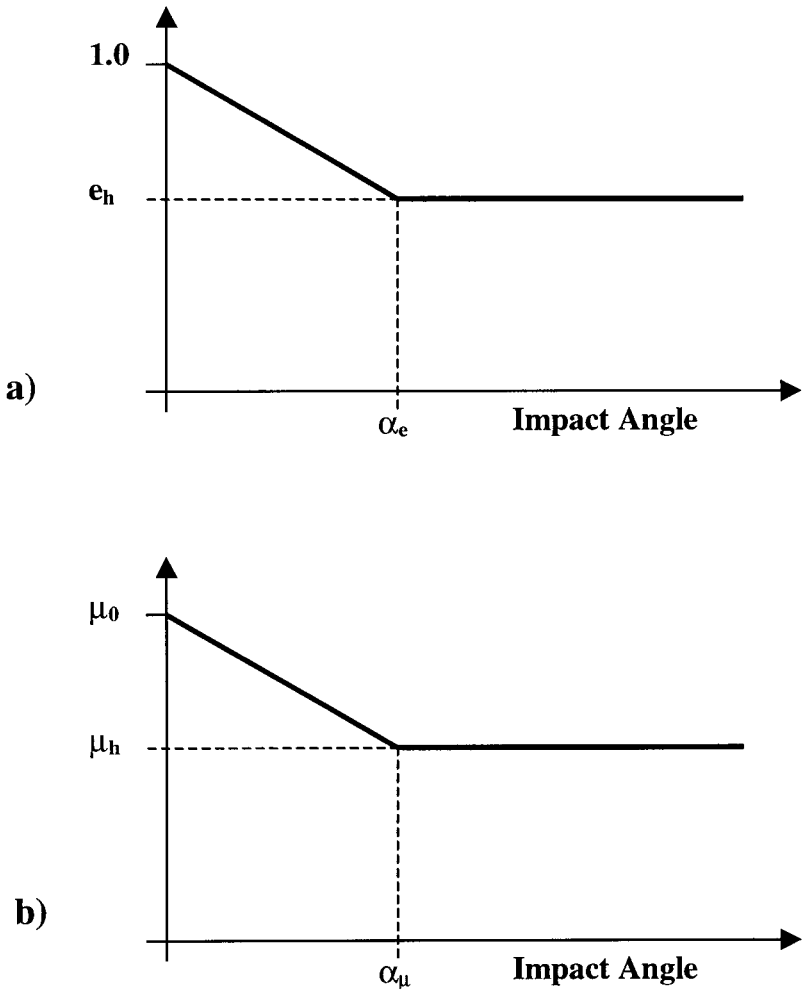

Fig. 20. Assumed variation of: (a) the restitution coefficient e, and (b) the friction coefficient with impact angle and characteristic values (see Table 1).

component is strongly influenced by the direction of rotation. For particles coming from the upper wall which have a negative rotation, the velocity ratio continuously decreases with increasing impact angle and becomes even negative for impact angles close to 90° for the considered mean angular velocity of −30.000 1/s. This implies that the particles are rebound backward due to the high angular momentum. For positive values of the angular velocity the velocity ratio is identical with that for negative angular velocity up to an impact angle of about 37.5° and then begins to increase with increasing impact angle. Close to 90° the velocity ratio becomes even larger than 1, i.e. the particle is rebound with a larger horizontal velocity since angular momentum is transformed to linear momentum. Angular mean velocities between ±30.000 1/s would give a velocity ratio between the two curves shown in Fig. 24(b). From this result it is obvious that rotation also affects the rebound angle for impact angles larger than

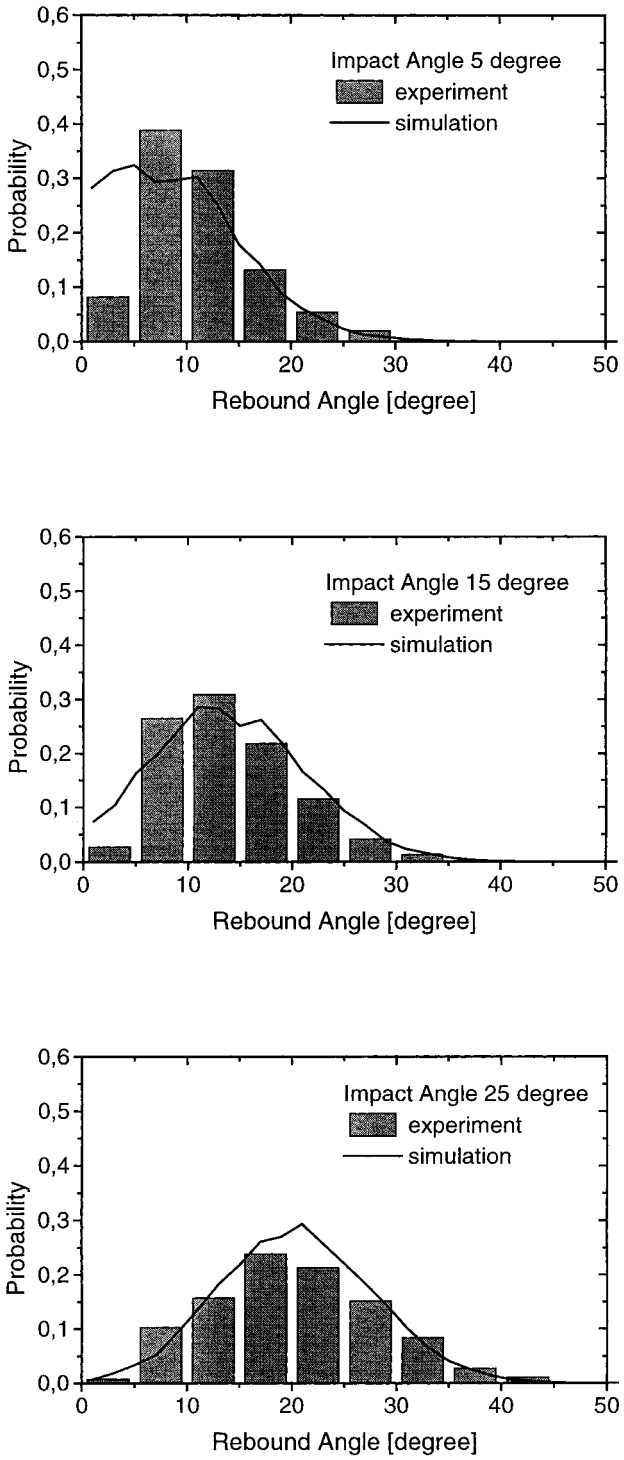

Fig. 21. Comparison of measured and simulated distributions of the rebound angle for different impact angles, 500 μm glass beads colliding on a stainless steel wall.

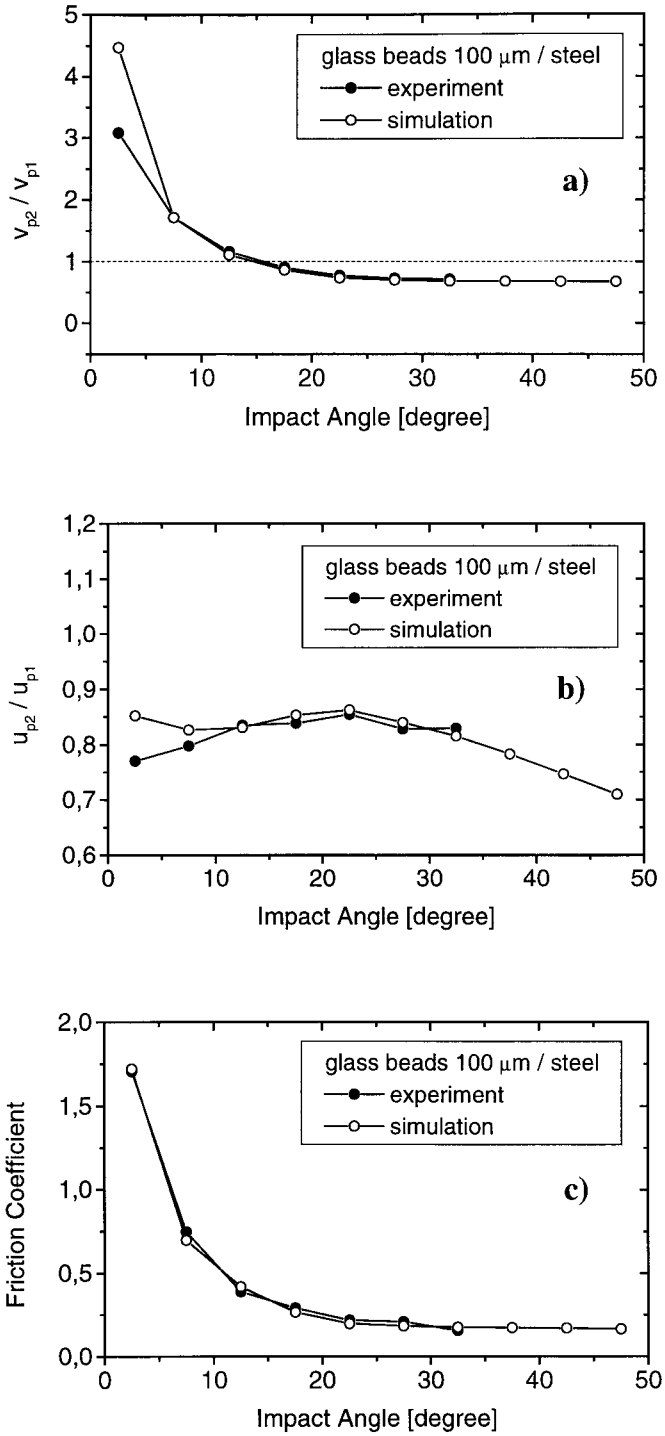

Fig. 22. Comparison of measured and simulated dependence of the velocity ratio normal to the wall (a), the velocity ratio parallel to the wall (b), and the friction coefficient (c) on the impact angle, 100 μm glass beads colliding on a stainless steel wall.

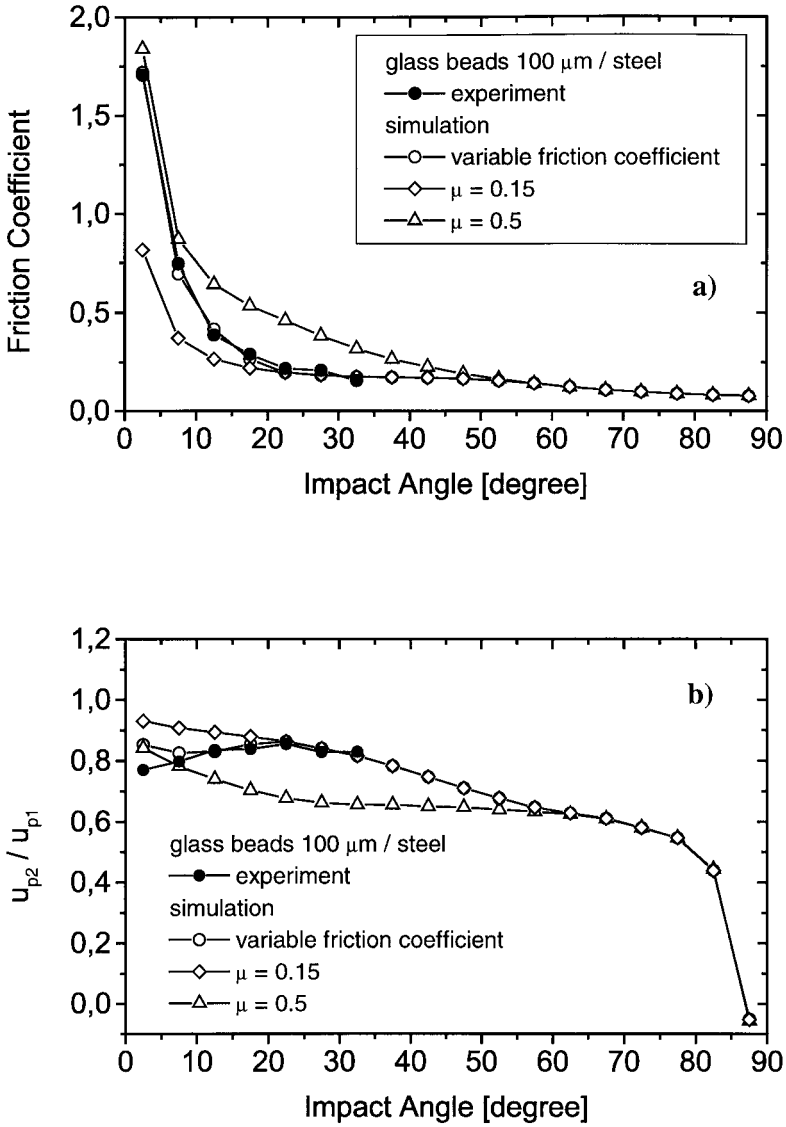

Fig. 23. Influence of the presumed dependence of friction coefficient on rebound characteristics as a function of impact angle, (a) friction coefficient, (b) velocity ratio parallel to the wall, (100 μm glass beads colliding with a stainless steel wall).

37.5°. For negative rotation the rebound angle becomes larger than for positive rotation (Fig. 24(c)). The agreement between measurement and simulation for the smooth wall and the 100 μm glass beads is very good for all the values discussed above (Fig. 24).

Finally, the case of the 100 μm glass beads and the rubber wall is considered (Fig. 25). For simulations with the parameters given in Table 1 a very good agreement is obtained with the measurement as demonstrated by comparing the rebound angle versus impact angle (Fig. 25(a)) and the velocity ratio parallel to the wall (Fig. 25(b)).

7. Conclusions

Wall roughness and non-sphericities of particles have a considerable influence on the wall collision process and the rebound properties of the particles. Aiming at improving a wall collision model to be implemented in a Lagrangian approach for the particle phase, a detailed experimental analysis of the wall collision process in a horizontal channel flow for different particles and wall materials was performed. The experiments revealed that both effects (i.e. wall

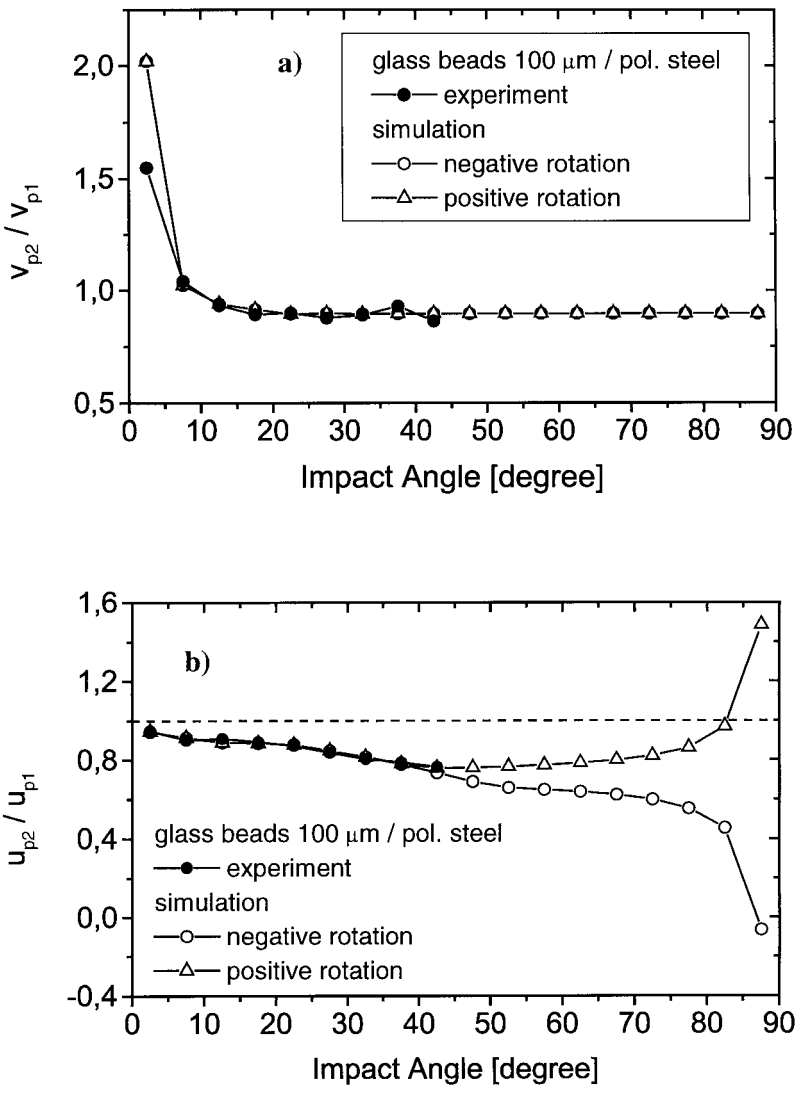

Fig. 24. Influence of particle rotation on rebound characteristics as a function of impact angle, (a) velocity ratio normal to the wall, (b) velocity ratio parallel to the wall, and (c) rebound angle, (100 μm glass beads colliding with a polished stainless steel wall).

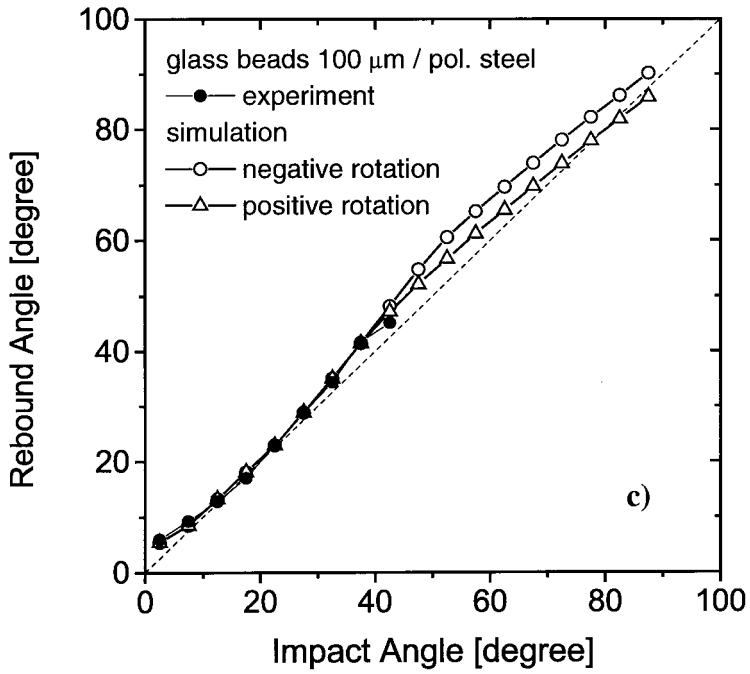

Fig. 24 (*continued*)

roughness and the non-sphericity of particles) yield in average for small impact angles a rebound of the particles at a larger angle. This phenomenon is a result of the so-called shadow effect which is associated with the fact that particles hit a roughness structure with a positive inclination with a higher probability. Regions on the lee-side of the roughness structure may not be hit at all for such small impact angles (i.e. impact angles below about 10°). The modelling of the wall roughness effect requires the consideration of this shadow effect. By optically scanning the stainless steel plate used in the experiments, it was found that the roughness angle distribution may be approximated by a normal distribution function with a standard deviation depending on the particle size. This standard deviation, which is an additional parameter in the wall collision model, was derived by using an analytic expression for the effective wall roughness angle distribution accounting for the shadow effect. Moreover, the dependence of the restitution coefficient and the friction coefficient on the impact angle could be derived from the experimental data. Since the wall collision process was calculated by solving the momentum equations in connection with Couloumbs law of friction these correlations are essential model parameters. Wall roughness was simulated by adding a stochastic component to the particle impact angle. For validating the developed wall collision model, a series of simulations were performed and the results were compared with the experimental data. The effect of the assumed dependence of the model parameters on the impact angle was analysed. The comparison of the model calculations with the experimental results showed a very good agreement for the different combinations of particle and wall material.

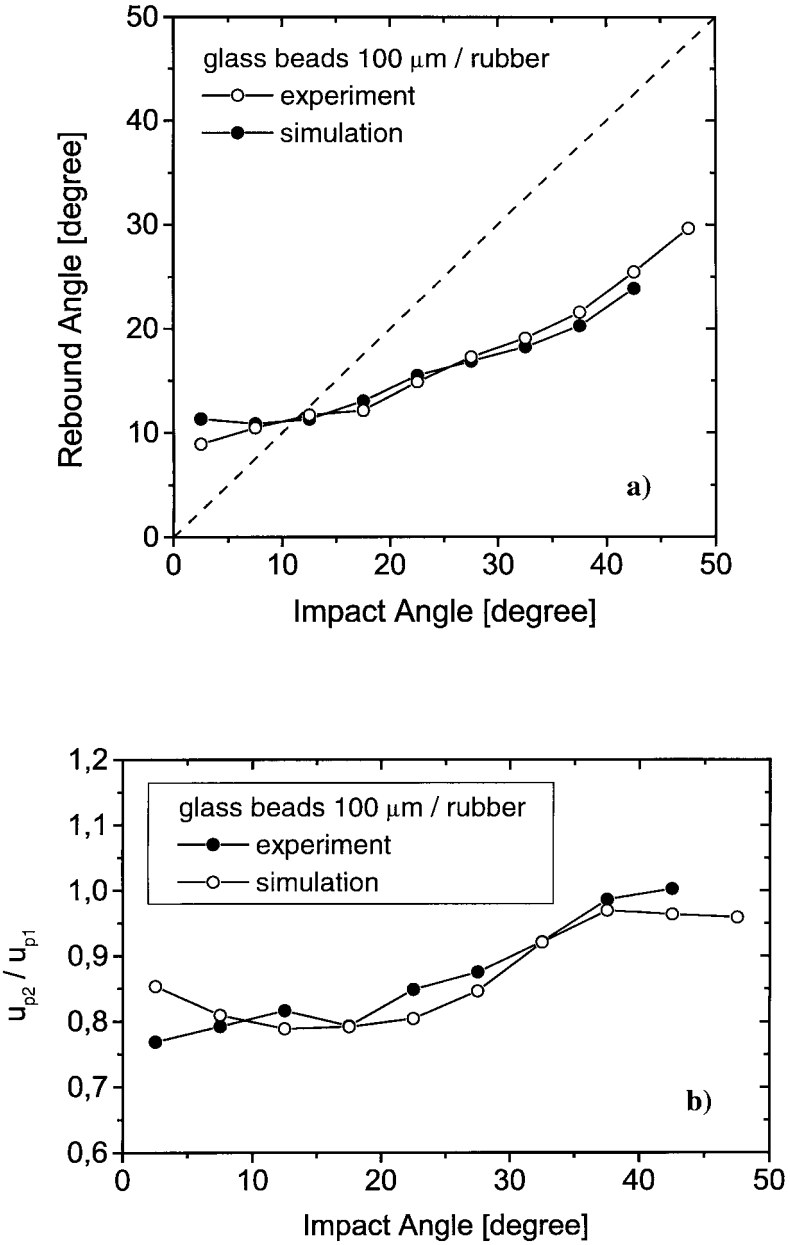

Fig. 25. Comparison of measurement and simulation for 100 μm glass beads colliding on a rubber wall, (a) rebound angle as a function of impact angle, (b) velocity ratio parallel to the wall versus impact angle.

Acknowledgements

The experimental studies were financially supported by the European Commission under contract No. 7220-ED/036 and the theoretical analysis and model developments were performed in the frame of a project supported by the Deutsche Forschungsgemeinschaft under contract No. 204/12-1.

References

Frank, Th., Schade, K.-P., Petrak, D., 1993. Numerical simulation and experimental investigation of a gas-solid two-phase flow in a horizontal channel. Int. J. Multiphase Flow 19, 187–198.

Grant, G., Tabakoff, W., 1975. Erosion prediction in turbomachinery resulting from environmental solid particles. J. Aircraft 12, 471–478.

Kulick, J.D., Fessler, J.R., Eaton, J.K., 1994. Particle response and turbulence modification in developed channel flow. J. Fluid Mech. 277, 109–134.

Martin, S.R., Pinfold, T.M., Wallace-Sims, G.R., 1991. LDA measurements of plastic and elastic collisions of small particles with metal surfaces. In: Adrain, R.J., Durao, D.F.G., Durst, F., Maeda, M., Whitelaw, J.H. (Eds.), Applications of Laser Techniques to Fluid Mechanics. Springer–Verlag, Berlin, pp. 125–141.

Schade, K.-P., Erdmann, H.-J., Petrak, D., 1996. Experimental investigation of the particle-wall collision under particular consideration of the wall roughness. In: Fluids Engineering Division Conference, ASME FED-236, 759–766.

Schade, K.-P., Hädrich, Th., 1998. investigation of influence of wall roughness on particle-wall collision. In: Third International Conference on Multiphase Flow, ICMF '98, Lyon, France, June 8–12.

Shaffer, F., Massah, H., Sinclair, J., Shahnam, M., 1994. Measurement of time-averaged particle wall collision properties using particle tracking velocimetry. In: Preprints First International Particle Technology Forum, Denver, CO, Part II, 499–504.

Sommerfeld, M., 1992. Modelling of particle/wall collisions in confined gas-particle flows. Int. J. Multiphase Flow 18, 905–926.

Sommerfeld, M., 1995. The importance of inter-particle collisions in horizontal gas-solid channel flows. In: Stock, D.E., Reeks, M.W., Tsuji, Y., Michaelides, E.E., Gautam, M. (Eds.), Gas-Particle Flows, ASME Fluids Engineering Conference, Hiltons Head, USA, ASME, FED–vol. 228, pp. 335–345.

Sommerfeld, M., 1996. Modellierung und numerische Berechnung von partikelbeladenen turbulenten Strömungen mit Hilfe des Euler/Lagrange-Verfahrens, Habilitaionsschrift, Universität Erlangen-Nürnberg, Shaker Verlag, Aachen.

Sommerfeld, M., Huber, N., Wächter, P., 1993. Particle-wall collisions: Experimental studies and numerical models. In: Stock, D.E., Reeks, M.W., Tsuji, Y., Gautam, M., Michaelides, E.E., Jurewicz, J.T. (Eds.), Gas–Solid Flows 1993, ASME Fluids Engineering Conference, Washington DC, FED–vol. 166, pp. 183–191.

Sommerfeld, M., Huber, N., 1995. A laser strobe technique combined with digital image analysis to study particle-wall collisions. In: Xu, Y., Wang, S. (Eds.), Modern Measuring Techniques for Multiphase Flows. Proceedings of the International Symposium on Measurement Techniques for Multiphase Flows, Nanjing, China, April 1995, pp. 428–440.

Sommerfeld, M., Zivkovic, G., 1992. Recent advances in the numerical simulation of pneumatic conveying through pipe systems. In: Hirsch, Ch., Periaux, J., Onate, E. (Eds.), Computational Methods in Applied Science. Invited Lectures and Special Technological Sessions of the First European Computational Fluid Dynamics Conference and the First European Conference on Numerical Methods in Engineering, Brussels, pp. 201–212.

Tsuji, Y., Morikawa, Y., Tanaka, T., Nakatsukasa, N., Nakatani, M., 1987. Numerical simulation of gas–solid two-phase flow in a two-dimensional horizontal channel. Int. J. Multiphase Flow 13, 671–684.

Tsuji, Y., Oshima, T., Morikawa, Y., 1985. Numerical simulation of pneumatic conveying in a horizontal pipe. KONA 3, 38–51.

Tsuji, Y., Shen, N.Y., Morikawa, Y., 1991. Lagrangian simulation of dilute gas–solid flows in a horizontal pipe. Adv. Powder Technol. 2, 63–81.